Journal of Heat and Mass Transfer Research 13 (2026), Serial Number 27, 367 – 386

Semnan University

Journal of Heat and Mass Transfer Research

Journal homepage: https://jhmtr.semnan.ac.ir

ISSN: 2383-3068

Research Article

Numerical Investigation of Convective Heat Transfer Effect on Divergent Shock Waves in Ideal Magnetogasdynamics

Kinakkal Athira [a] , Dunna Narsimhulu [a*], Devarapalli Nagendra Prasad [b]

[a] *Department of Statistics and Applied Mathematics, Central University of Tamil Nadu, Neelakudi, Thiruvarur-610 005, Tamil Nadu, India*

[b] *Department of Physics, Vallurupalli Nageswara Rao Vignana Jyothi Institute of Engineering and Technology (VNR-VJIET), Bachupally, Hyderabad-500090, Telangana, India*

ARTICLE INFO

Article history:

Received: 2024-09-25

Revised: 2025-06-12

Accepted: 2025-07-24

Keywords:

Shock wave;

Similarity solution;

Ideal gas equation of state;

Magnetogasdynamics (MGD);

Convective heat transfer.

ABSTRACT

This study examines the impact of heat transfer mechanisms such as conduction, radiation and convection, on the propagation of spherical and cylindrical shock waves generated by the motion of a piston in an ideal magnetohydrodynamic (MHD) gas at equilibrium. The thermal properties of the medium, including its heat transfer capacity and absorption coefficient, are influenced by temperature variations. The governing equations are expressed in the form of a coupled system of nonlinear partial differential equations in the Eulerian framework, with the incorporation of multiple heat transfer modes. Key flow parameters such as velocity, density, pressure, magnetic pressure and total energy are analyzed to understand the behavior of the shock wave under varying conditions. The findings of the study demonstrate that the piston velocity index, magnetic field intensity, and the convective heat transfer parameters such as convective coefficient (h^*), Nusselt number, and characteristic length significantly affect the shock strength and flow dynamics. Notably, pressure and energy distributions exhibit a strong dependence on (h^*). Moreover, it is evident from observations that the interaction between shock dynamics and heat transfer is significantly influenced by the system's geometry. The obtained results of the study align well with established literature reports.

1. Introduction

The behavior of shock waves in an ideal gas is a crucial area of study due to its potential applications in photo-ionized gas, inertial confinement fusion (ICF) experiments, star formation, shock wave physics, magnetogasdynamics generators, material synthesis and processing, hypersonic propulsion, core-collapse supernovae, magnetic field amplification, shock-induced instabilities, the collision of ionized cloud of gas, medical treatments, shock wave lithotripsy, shock wave therapy, etc. [1]. Shock waves propagate at supersonic speeds and exhibit non-linear behavior. They are characterized by a rapid and dramatic increase in pressure, dissipation of energy, and rapid changes in velocity, temperature, and density. In the 19th century, Ernst Mach, the Austrian physicist and philosopher, significantly contributed to the study of shock waves. He investigated the behavior of shock waves in supersonic flows and formulated the Mach number, which describes

* **Corresponding author.**
E-mail address: narsimha.maths@gmail.com

Cite this article as:

Athira, K., Narsimhulu, D. and Prasad, D.N., 2026. Numerical Investigation of Convective Heat Transfer Effect on Divergent Shock Waves in Ideal Magnetogasdynamics. *Journal of Heat and Mass Transfer Research*, 13(3), pp. 367-386.

https://doi.org/10.22075/JHMTR.2025.35432.1611

the ratio of the speed of an object to the local speed of sound. His work laid the foundation for understanding compressible flow and shock wave physics [2, 3].

The first theoretical explanation of the intensification and scaling behavior near the point of convergence was given by Guderley [4], who derived self-similar solutions for strong spherical and cylindrical shock waves converging toward a central point or axis. Chester [5], Chisnell [6], and Whitham [7] all carried out independent investigations of the same problem with a focus on geometrical shock dynamics. Gurovich et al. [8] investigated semi-analytical solutions to the well-known problem of strong convergent shock waves in an ideal gas. Sharma and Arora [9] approached the problem of an imploding shock wave in an ideal gas using the Lie group-theoretic method with constant surface conditions. Convergent shock waves were investigated by Hafner [10] in a quiescent ideal gas at zero pressure. Van Dyke and Guttmann [11] used a perturbation series approach to study an implosion problem in an ideal gas with constant density. The work of Van Dyke and Guttmann was further expanded by Madhumita and Sharma [12], who included the consideration of an ideal gas whose density varied with respect to time and space. Levin and Zhuravskaya [13] investigated the behavior of converging and diverging spherical and cylindrical shock waves in perfect gas flow under isothermal conditions.

Investigating the behavior of shock wave propagation under the influence of a magnetic field for an ideal gas is essential, as ideal magnetogasdynamics flow involves a plasma. Bertram [14] published the first comprehensive shock solution while studying the one-dimensional steady flow of an ideal gas in magnetogasdynamics. Singh et al. [15] studied the propagation of a weak shock wave under the influence of a magnetic field in an electrically conducting inviscid flow. By adopting the radiation diffusion approximation, Marshak [16] investigated the impact of radiation on shock propagation. The importance of studying heat transfer phenomena in different media, such as ideal, non-ideal, dusty gas, nanofluids, and porous media, with the effects of gravitational, viscous dissipation, magnetic, etc., has received significant attention in recent times. Although the literature has extensively discussed shock wave similarity solutions in a perfect gas, prior works did not address the effect of the modes of heat transfer in ideal magnetogasdynamics. The modes of heat transfer collectively have not been taken into consideration in the existing literature.

Recently, Bajargaan and Patel [17] and Nath [18] have considered the effect of heat conduction and radiation heat flux in gas medium. With respect to existing literature and the authors' knowledge, no reports have been communicated on the collective impact of all three modes of heat transfer in a single study, especially in relation to the magnetic field effect in an ideal gas. Nath and Vishwakarma [19, 20] reported the influence of heat transfer modes by assuming the medium to be a non-ideal gas. In recent years, shock wave studies in magnetogasdynamics [31,32] have drawn more attention due to their relevance to modern propulsion systems, high-temperature plasma flows at high speeds, and various astrophysical phenomena.

A thorough understanding of the convection process in shock wave phenomena is critical due to its broad range of practical applications [33-36]. For instance, i) shock waves are generated during the rapid passage of supersonic and hypersonic flight through the atmosphere. Designing heat shields and controlling the extreme temperatures encountered during re-entry into the Earth's atmosphere requires a thorough understanding of convection and heat transfer; ii) shock waves are produced by projectiles or bullets traveling at supersonic speeds in weapons like guns and artillery. This may have an impact on the overall performance and accuracy of weapons. To regulate the heat produced during the firing process and to provide efficient cooling systems for barrels, convection studies are used; iii) Shock waves in chemical reactors can result from exothermic reactions or high-pressure flow. Understanding convection and heat transfer is essential for controlling and optimizing these processes to ensure their effectiveness and safety; iv) Atmospheric shock waves, such as thunderstorms or volcanic eruptions, can cause severe weather occurrences. Meteorologists can more accurately predict the weather by understanding the heat transfer processes involved in these phenomena; v) nuclear explosions and reactor mishaps result in shock waves and extremely high temperatures. Understanding convection is crucial for forecasting the behavior of materials and fluids in these conditions and assessing the safety of nuclear reactors.

This paper examines how heat transfer mechanisms of a spherical and cylindrical strong divergence (explosion) problem propagate in an ideal gas EoS regime, affecting the strength of the axial or azimuthal magnetic field generated by a moving piston that drives the shock wave.

The heat transfer mechanism has a significant impact on determining the overall thermodynamic behavior of the fluid during the propagation of a shock wave. Studying the combined effect of conduction, convection, and radiation is more crucial than considering only the effect of conduction and radiation in shock wave problems because the presence of convective heat transfer can considerably alter the behavior and attributes of shock waves. Nevertheless, this is the first time we have included the combined effect of all these factors on flow variables in an ideal gas in relation to the magnetic field in spherical and cylindrical cases. In the perfect gas EoS, the physical behavior of shock wave properties such as density, velocity, pressure, magnetic pressure, and energy is examined in both spherical and cylindrical cases. The influence of both convection and non-convection processes on these properties is also examined.

2. Mathematical Modelling of Piston Problem

2.1. Physical Model

A tightly fitted piston is suddenly forced into a gas at constant velocity v_p, contained within a uniform tube at the time $t = 0$. As the piston moves, a compression wave is generated that propagates through the gas with speed W_f. When the velocity of the piston exceeds the velocity of sound in the gas, a shock wave is produced, a sharp front in which the properties of the gas rapidly change. The gas is compressed behind the shock wave, increasing its pressure and density while decreasing its velocity. Assume that the piston is at rest ($s = 0$, $t = 0$) and is moving in the positive s-direction. Consequently, there occur two different gas zones in the medium. This can be seen from the Fig. 1.

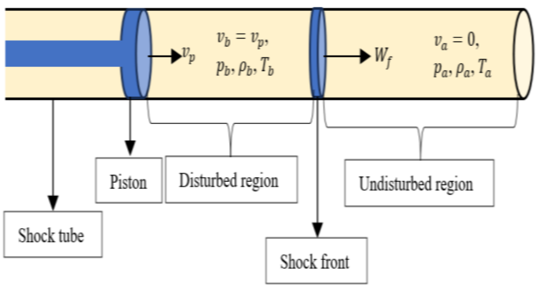

Fig. 1. Schematic diagram for the piston problem

- *Undisturbed region:* The gas is not disturbed in the area to the right side of the shock wave. Therefore, $v_a = 0$ is the velocity and p_a, ρ_a, and T_a are pressure, density, and temperature ahead of the shock wave, respectively.
- *Disturbed region:* The gas is between the piston and the shock wave, which is moving at the same speed as the piston velocity. It has a velocity $v_b = v_p$ and p_b, ρ_b, and T_b are pressure, density, and temperature behind the shock wave, respectively.

The propagation of a shock wave produced by a moving piston in a medium with either spherical or cylindrical symmetry is examined in this work. The radial distance from the center (for spherical symmetry) or the axis of symmetry (for cylindrical symmetry) is represented by the coordinate s. The center of the sphere or the axis of the cylinder is taken as the origin of the coordinate system, and the center of the shock front propagation is assumed to be the origin of the magnetic field generation. In both spherical and cylindrical coordinate systems, it is assumed that there is an axial magnetic field oriented along a fixed direction (such as the z-axis). To maintain uniformity in the formulation of the coordinate system and the magnetic field throughout the analysis, the governing equations are developed assuming either spherical or cylindrical symmetry and an azimuthal, axial magnetic field. Since the axial magnetic field is aligned with the symmetry axis, it can only maintain a perpendicular orientation relative to the shock front at the equatorial plane (or great circle), thereby limiting its impact to this specific region. In contrast, the azimuthal magnetic field, which encircles the axis, remains orthogonal to the radial flow lines across a significantly larger portion of the shock surface. This configuration ensures that magnetic influences persist over an extensive area of the shock front. As a result, the interplay between both magnetic field components creates a composite geometry that permeates the domain, allowing meaningful interaction with fluid dynamics. This extended interaction reinforces the solutions' applicability beyond a single plane, ensuring broader validity.

2.2. Mathematical Description of Solution Methodology

The solution method involves generating the equations governing the motion of the compressible flow based on the nature of the problem considered and the assumptions made, as well as defining the applicable initial and boundary conditions and the medium into which the shock propagates. These highly non-linear PDEs of Poincare type are challenging to obtain analytical solutions. For applying suitable self-similarity transformations, the governing equations are transformed into a system of ODEs. The solution methodology for the defined problem involves the following steps:

- The governing PDEs and suitable boundary conditions are introduced.
- Reduce PDEs into ODEs using similarity transformations, emphasizing the assumption of self-similarity of the first kind.
- Governing equations are transformed into a non-dimensional form using characteristic scales for variables like velocity, density, pressure, magnetic field, and energy.
- Based on the solution behavior, appropriate boundary conditions, were applied, and the resulting ODEs were solved using the fourth-order Runge-Kutta method.

2.3. Basic Equations and Boundary Conditions

The fundamental equations for governing the motion of one-dimensional unsteady compressible flow, considering the effects of conductive, radiative, and convective heat fluxes in an ideal magnetogasdynamics regime, can be written as [18, 19, 20].

$$\frac{\partial\rho}{\partial t}+\frac{\partial(\rho v)}{\partial s}+\frac{\lambda v\rho}{s}=0 \tag{1}$$

$$\frac{\partial v}{\partial t}+v\frac{\partial v}{\partial s}+\frac{1}{\rho}\left(\frac{\partial p}{\partial s}+\frac{\partial h}{\partial s}\right)+\frac{2mh}{\rho s}=0 \tag{2}$$

$$\frac{\partial h}{\partial t}+\frac{\partial(vh)}{\partial s}+h\frac{\partial v}{\partial s}+\frac{2hv\eta}{s}=0 \tag{3}$$

$$\frac{\partial e}{\partial t}+v\frac{\partial e}{\partial s}-\frac{p}{\rho^2}\left(\frac{\partial\rho}{\partial t}+v\frac{\partial\rho}{\partial s}\right)+\frac{1}{\rho s^\lambda}\frac{\partial}{\partial s}\left(Fs^\lambda\right)=0 \tag{4}$$

where h is defined by $h=\frac{\mu H^2}{2}$, H represents the strength of the magnetic field, which can be either axial or azimuthal, and μ is assumed to be equal to one. The dimensionless constants $\lambda\,(=1,2)$, $m\,(=0,1)$, $\eta\,(=0,1)$ describe the geometry of the shock wave and magnetic field. $\lambda=1$indicates a cylindrically symmetric shock wave, and $\lambda=2$ indicates a spherically symmetric shock wave. The values of m and η represents the magnetic field configuration. $m=1$ for the presence and $m=0$ for the absence of an azimuthal magnetic field. Similarly, $\eta=0$ for the absence, $\eta=1$ for the presence of the axial magnetic field.

In equation (1), the terms $\frac{\partial\rho}{\partial t}$ (local density change term), $\frac{\partial(\rho v)}{\partial s}$ (convective term) are essential for capturing the unsteady behavior and movement of mass within the fluid; the $\frac{\lambda v\rho}{s}$ (symmetry term), ensures the consistency of the equation with the geometry of the flow. In equation (2), the terms $\rho\left(\frac{\partial v}{\partial t}+v\frac{\partial v}{\partial s}\right)$ (inertial term), $\frac{\partial(p+h)}{\partial s}$ (pressure gradient) are crucial for understanding the dynamics of the fluid and the balance of forces; the magnetic force term $\frac{2mh}{\rho s}$, which includes the azimuthal magnetic field effects in the fluid motion. In equation (3), $\frac{\partial h}{\partial t}$ (temporal change term) is essential for capturing the unsteady magnetic effect, and $\frac{2hv\eta}{s}$ (axial magnetic field term) guarantees the axial magnetic field effect being included in the spherical and cylindrical symmetry; the term $\frac{\partial(vh)}{\partial s}+h\frac{\partial v}{\partial s}$, which is the combination of $v\frac{\partial h}{\partial s}$ (advection) and $2h\frac{\partial v}{\partial s}$ (velocity gradient interaction), is important for understanding the movement of the magnetic field through the fluid and for capturing the attenuation of the magnetic field with respect to velocity change. In equation (4), the term $\frac{\partial e}{\partial t}$ (temporal change term), $v\frac{\partial e}{\partial s}$ (convective transport term) give a clear picture of transient energy behavior and how the energy moves with the fluid flow; the term $-\frac{p}{\rho^2}\left(\frac{\partial\rho}{\partial t}+v\frac{\partial\rho}{\partial s}\right)$ (pressure work) is important for understanding how pressure forces affect the internal energy, and $\frac{1}{\rho s^\lambda}\frac{\partial}{\partial s}\left(Fs^\lambda\right)$ (flux term) allows for addition or loss of energy in the model.

The system of governing equations (1-4) is supplemented by the following EoS [24]:

$$p=\rho R^*T \tag{5}$$

The above equation can be rewritten as:

$$e=\frac{p}{\rho(\gamma-1)} \tag{6}$$

In the presence of an azimuthal or axial magnetic field, we suppose that a diverging spherical or cylindrical shock wave is propagating outward from the point or axis of symmetry in the undisturbed medium with a constant initial density. Consequently, the flow parameters just before the shock front are as follows [21].

$$\begin{aligned}&v=v_a=0, &&\rho=\rho_a=\text{constant},\\&H=H_a=H^*{s_b}^{-\varepsilon}, &&F=F_a=0\end{aligned} \tag{7}$$

The expression for total heat flux in equation (4) can be decomposed into the following form:

$$F=F_{Cd}+F_{Rd}+F_{Cn} \tag{8}$$

Fourier's law of heat conduction states that [24]

$$F_{Cd}=-k\frac{\partial T}{\partial s} \tag{9}$$

The diffuse radiation model predicts that in an optically thick gray gas, the flow's local thermodynamic equilibrium conditions are preserved [22]. The radiative gas's radiation heat fluxes (F_{Rd}) can be calculated using the differential approximation of the radiation transfer equation in the diffusion limit. The equation for this can be written as follows [24]:

$$F_{Rd} = -\frac{4}{3}\left(\frac{\sigma}{\alpha_R}\right)\frac{\partial T^4}{\partial s} \tag{10}$$

According to Newton's law of cooling, thermal heat convection is expressed by the relation [24].

$$F_{Cn} = h^* \frac{\partial T}{\partial s} \tag{11}$$

The coefficient of thermal conductivity k, the absorption coefficient α_R, and the coefficient of convective heat transfer h^* are considered to change depending on density and temperature. These can be expressed by the following power laws [19, 23, 24].

$$k = k_0\left(\frac{T}{T_0}\right)^{\beta_c}\left(\frac{\rho}{\rho_0}\right)^{\delta_c} \tag{12}$$

$$\alpha_R = \alpha_{R_0}\left(\frac{T}{T_0}\right)^{\beta_R}\left(\frac{\rho}{\rho_0}\right)^{\delta_R} \tag{13}$$

$$h^* = \frac{N_u}{L}k_0\left(\frac{T}{T_0}\right)^{\beta_c}\left(\frac{\rho}{\rho_0}\right)^{\delta_c} \tag{14}$$

The exponents β_c, β_R, δ_c, and δ_R are dimensionless constants, that are established using gas properties at the suitable temperature range.

2.4. *Rankine*–Hugoniot jump conditions

The Rankine-Hugoniot jump conditions can be expressed mathematically as a set of equations relating the fluid parameters ahead (upward region) and behind (downward region) the shock front as the shock wave propagates through the medium. The conservation of mass, magnetic field, momentum, and energy across the shock front can be written as follows:

$$\begin{gathered}\rho_a W_f = \rho_b(W_f - v_b)\\ h_a W_f = h_b(W_f - v_b)\\ p_a + h_a + \rho_a {W_f}^2 = p_b + h_b + \rho_b(W_f - v_b)^2\\ e_a + \frac{p_a}{\rho_a} + \frac{1}{2}{W_f}^2 + \frac{\mu h_a}{\rho_a} = e_b + \frac{p_b}{\rho_b} + \frac{1}{2}(W_f - v_b)^2 + \frac{\mu h_b}{\rho_b} - \frac{F_b}{\rho_a W_f}\end{gathered} \tag{15}$$

Using equations (6) and (15), the R-H conditions for a shock front in a perfect gas can be written as

$$\begin{gathered}\rho_b = \frac{\rho_a}{\beta},\ v_b = (1-\beta)W_f,\ h_b = \frac{h_a}{\beta},\\ p_b = \left[(1-\beta) + C_a\left(1-\frac{1}{\beta}\right) + \frac{1}{\gamma M^2}\right]\rho_a {W_f}^2\\ F_b = (1-\beta)\left[\left(\beta - c_a + \frac{1}{\gamma M^2}\frac{\beta}{(\beta-1)}\right)\frac{\gamma}{(\gamma-1)} + \frac{(1+\beta)}{2}\right]\rho_a {W_f}^3\end{gathered} \tag{16}$$

where $M = \left(\frac{\rho_a {W_f}^2}{\gamma p_a}\right)^{\frac{1}{2}}$ and $C_a = \left(\frac{h_a}{\rho_a {W_f}^2}\right)$

A shock front has an abrupt change in pressure, velocity, or temperature as a fluid spreads through a medium. The velocity at which the shock front propagates through the fluid is defined as the shock front speed. When a fluid undergoes a quick change, such as compression or expansion, a shock wave is generated and travels with the fluid within the medium. The speed of a shock wave is determined by fluid parameters such as density and viscosity, as well as the degree (magnitude) and duration of the abrupt change.

Substituting equations (6) and (16) into equation (15), the quadratic relation that provides the density ratio β $(0 < \beta < 1)$ over the shock front is given by:

$$\beta^2 - \beta\left[C_a + \frac{1}{\gamma M^2}\right] - C_a = 0 \tag{17}$$

3. Self-Similar Solutions

The gas dynamic equations admit several group-theoretic transformations. These gas dynamic equations contain the five-dimensional quantities ρ, v, p, s, and t, and the dimensions of three of them are independent. These can be used to characterize the motion of the object itself by altering the fundamental length, time, and density scales. There are certain motions whose unique characteristic is their motions' resemblance. They are referred to as self-similar motions [25].

3.1. *Analysis of Reduced System of Equations*

We use suitable similarity transformations to reduce the basic equations along with the boundary conditions into a set of ordinary differential equations. The flow field's inner border behind the shock front is considered to be the expanding piston. The piston velocity is assumed to follow a power law within a self-similarity framework, as given by the following relation [19, 20].

$$v_p = \frac{ds_p}{dt} = V_0 \left(\frac{t}{t_0}\right)^n \tag{18}$$

constraints on n are imposed by considering ambient magnetic field and pressure (see equation (22)). This changes the piston movement from zero to infinity almost instantaneously, forming a high-energy initial shock. Consequently, the piston is then slowed down. The boundary conditions for the shock must be self-similar, so the velocity of the shock W_f, must be proportional to the velocity of the piston v_p as expressed by the given relation [19, 20]

$$W_f = \frac{ds_b}{dt} = CV_0 \left(\frac{t}{t_0}\right)^n \tag{19}$$

Using equation (19), we can convert time and space coordinates into non-dimensional variable y as follows.

$$y = \frac{s}{s_b} = \left[\frac{(n+1){t_0}^n}{CV_0}\right]^n \left(\frac{s}{t^{n+1}}\right) \tag{20}$$

The distribution of flow variables as a function of position and time, follows a self-similar motion. For instance, the motion of change in the pressure distribution (p) is altered by the pressure scale π and the length scale s_b of the shock wave region, but the shape of the pressure distribution remains constant. The expression for the function p is $p = \pi P(\frac{s}{s_b})$, and the dimensionless ratio $\frac{p}{\pi} = \pi(\frac{s}{s_b})$ is a universal function of the new dimensionless co-ordinate $y = \frac{s}{s_b}$. The true pressure distribution curve p as a function of location for any time t can be obtained from the universal function $\pi(y)$ by multiplying the scales π and y by the scale functions π and s_b. The density, velocity, magnetic pressure, and internal energy are defined in a similar way [25].

Thus, we get the conditions $y = y_p \left(= \frac{s_p}{s_b}\right)$ at the piston and $y = 1$ at the shock front. In order to obtain the similarity solution, the new flow variables (unknown variables) are formulated as follows [19, 20].

$$\begin{gathered} v = \frac{s}{t} V(y), \qquad p = \rho_a \frac{s^2}{t^2} P(y), \\ h = \rho_a \frac{s^2}{t^2} A(y),\ \rho = \rho_a D(y),\ F = \rho_a \frac{s^3}{t^3} Q(y) \end{gathered} \tag{21}$$

where V, P, D, A, and Q are new dimensionless functions of velocity (v), pressure (p), density (ρ), magnetic pressure (h), and total thermal heat flux (F), respectively. To ensure the existence of self-similar solutions, the parameters M and C_a remain constants; thus, we obtain the following condition:

$$\varepsilon = -\frac{n}{n+1} \tag{22}$$

The exponents in the aforementioned equations should meet the similarity requirements for a desired self-similar solution.

Using equations (9)-(14) in equation (8) (after a little algebra), we get,

$$F = \left[\left(\frac{N_u}{L} - 1\right) k_0 \left(\frac{T}{T_0}\right)^{\beta_C} \left(\frac{\rho}{\rho_0}\right)^{\delta_C} - \frac{16\,\sigma {T_0}^{\beta_R} {\rho_0}^{\delta_R}}{3\alpha_{R_0}} T^{3-\beta_R} \rho^{-\delta_R}\right] \frac{\partial T}{\partial s} \tag{23}$$

Similarity solutions of the chosen problem prevail [17, 21] only when:

$$\beta_C = 1 + \frac{1}{2n},\ \beta_R = 2 - \frac{1}{2n} \tag{24}$$

The above relationship (24) shows the impact of energy conversion due to the dependency of β_C and β_R on the index n.

Substitute equations (6), (21), and (24) in equation (23) to obtain:

$$Q = -Y\left[\frac{y^{\frac{1}{n}}}{D}\left(2P + y\frac{\partial P}{\partial y}\right) - y^{\frac{n+1}{n}} \frac{P}{D^2}\frac{\partial D}{\partial y}\right] \tag{25}$$

where

$$Y = \left[\Gamma_{Cd} D^{\delta_c - 1 - \frac{1}{2n}} + \Gamma_{Cn} D^{\delta_c - 1 - \frac{1}{2n}} + \Gamma_{Rd} D^{-\delta_R - 1 - \frac{1}{2n}}\right] \frac{(P)^{1+\frac{1}{2n}}}{(n+1)^{\frac{1}{n}}}.$$

where Γ_{Cd}, Γ_{Cn}, and Γ_{Rd} are conductive, convective, and radiative dimensionless heat transfer parameters, respectively. The parameters Γ_{Cd}, Γ_{Cn} depend on the thermal conductivity k, and Γ_{Rd} depends on $\frac{1}{\alpha_R}$, the mean free path of radiation, respectively, and also on the exponents n, and they are given by:

$$\begin{gathered} \Gamma_{Cd} = \frac{k_0 {\rho_a}^{\delta_c - 1}}{T_0 t_0 {\rho_0}^{\delta_C} {R^*}^2} \left(\frac{CV_0}{\sqrt{T_0 R^*}}\right)^{\frac{1}{n}}, \\ \Gamma_{Cn} = \frac{N_u}{L} \frac{k_0 {\rho_a}^{\delta_c - 1}}{T_0 t_0 {\rho_0}^{\delta_C} {R^*}^2} \left(\frac{CV_0}{\sqrt{T_0 R^*}}\right)^{\frac{1}{n}}, \\ \Gamma_{Rd} = \frac{16\sigma {T_0}^2 {\rho_0}^{\delta_R}}{3 t_0 {\rho_a}^{\delta_R + 1} {R^*}^2 \alpha_{R_0}} \left(\frac{CV_0}{\sqrt{T_0 R^*}}\right)^{\frac{1}{n}} \end{gathered} \tag{26}$$

The similarity transformations (21) are not arbitrary; rather, they are based on the assumption of self-similarity of the first kind. In this context, dimensional analysis and the intrinsic symmetry of the physical problem provide a framework for selecting the appropriate similarity variables. Similarity transformation (21) can be used to convert the system of fundamental equations (1-4) into a system of ODEs. Under the self-similarity assumption, the resulting ODEs form a distinct class of solutions that are consistent with the original PDEs.

The solutions derived in the similarity framework can therefore be transferred back to the original physical variables, and it is shown that they satisfy the original PDEs, even though the transformed systems appear simplified. This ensures the preservation of the original model's mathematical and physical integrity.

These reduced ODEs can be cast into the following matrix equation:

$$Gz = u \tag{27}$$

where $G = \begin{bmatrix} yD & a_{12} & 0 & 0 & 0 \\ a_{21} & 0 & y & y & 0 \\ 2yA & 0 & a_{33} & 0 & 0 \\ 0 & a_{42} & 0 & a_{44} & a_{45} \\ 0 & a_{52} & 0 & a_{54} & 0 \end{bmatrix}$

here $a_{12} = a_{33} = \big(V - (n+1)\big)y$,

$a_{21} = a_{44} = \big(V - (n+1)\big)yD$,

$a_{42} = \big(V - (n+1)\big)yP\gamma$,

$a_{45} = y(\gamma - 1)D$, $a_{52} = \frac{-2PYy^{1+\frac{1}{n}}}{D^2}$,

$a_{54} = \frac{-Yy^{1+\frac{1}{n}}}{D}$, and

$$u = \begin{bmatrix} (\lambda+1)VD \\ (V-1)DV + 2(1+m)A + 2P \\ 2AV(2+\eta) - 2A \\ 2DP(V-1) + (\gamma-1)D(3+\lambda)Q \\ \frac{-2PYy^{1+\frac{1}{n}}}{D^2} \end{bmatrix},$$

$$z = \begin{bmatrix} \frac{dV}{dy} & \frac{dD}{dy} & \frac{dA}{dy} & \frac{dP}{dy} & \frac{dQ}{dy} \end{bmatrix}^T$$

Using Cramer's rule to solve the above system (27) to obtain the derivatives of the reduced flow variables. These derivatives of the reduced flow variables are written in the following form:

$$\frac{dV}{dy} = \frac{\Delta_1}{\Delta}, \frac{dD}{dy} = \frac{\Delta_2}{\Delta}, \frac{dA}{dy} = \frac{\Delta_3}{\Delta}, \frac{dP}{dy} = \frac{\Delta_4}{\Delta}, \frac{dQ}{dy} = \frac{\Delta_5}{\Delta}$$

where

$$\frac{dV}{dy} = \frac{1}{J}\left[\left(\frac{1}{y}\right)\big(V-(n+1)\big)\left[DV(V-1) + 2(1+m)A + \frac{[2A-(2+\eta)2VA]}{y[V-(n+1)]}\right] - \frac{QD}{Yy^{1+\frac{1}{n}}}[V-(n+1)]\frac{(\lambda+1)PV}{y}\right], \tag{28}$$

$$\frac{dD}{dy} = -\frac{D}{[V-(n+1)]}\left[\frac{dV}{dy} - \frac{(\lambda+1)V}{y}\right], \tag{29}$$

$$\frac{dA}{dy} = \frac{2A}{y[V-(n+1)]}\left[1 - (2+\eta)V - y\frac{dV}{dy}\right], \tag{30}$$

$$\frac{dP}{dy} = \frac{1}{y}\left[\left(\frac{2A}{[V-(n+1)]} - [V-(n+1)]D\right)y\frac{dV}{dy} - (V-1)DV - 2(1+m)A - 2P - \frac{2A}{[V-(n+1)]}\big(1+(2+\eta)V\big)\right], \tag{31}$$

$$\frac{dQ}{dy} = \frac{[[V-(n+1)]^2D - 2A]}{(\gamma-1)}\frac{dV}{dy} - \frac{\gamma P}{(\gamma-1)}\frac{dV}{dy} - \frac{(\lambda+1)V\gamma P}{y(\gamma-1)} - \frac{(3+\lambda)Q}{y} + \frac{2}{y(\gamma-1)}[A - (2+\eta)VA - P(V-1)] + \frac{[V-(n+1)]}{y(\gamma-1)}[(V-1)DV + 2P + 2(1+m)A]. \tag{32}$$

where

$$J = J(y) = [\{2A - [V-(n+1)]^2D\} + P]$$

3.2. Transformed Boundary Conditions

Flow variables such as pressure, density, temperature, and velocity change rapidly within fluid dynamics across the shock front. These changes are governed by conservation laws such as conservation of mass, momentum, and energy. Boundary conditions are the values of flow variables at the interface between the shocked and unshocked parts of the shock wave. Conservation laws are used to derive these relationships across the front of the shock wave. The R-H jump relations that connect the flow variables on both sides of the shock front are the most important boundary conditions for the shock front.

Applying the transformations (21) to the R-H conditions (16) yields the transformed boundary conditions at the shock front. These can be written in the following form:

$$\begin{aligned} &V(1) = (1-\beta)(n+1), \quad D(1) = \frac{1}{\beta}, \\ &A(1) = \frac{C_a}{\beta}(n+1)^2, \\ &P(1) = \left[(1-\beta) + C_a\left(1 - \frac{1}{\beta}\right) + \frac{1}{\gamma M^2}\right](n+1)^2 \\ &Q(1) = (1-\beta)\left[\left(\beta - c_a + \frac{1}{\gamma M^2}\frac{\beta}{(\beta-1)}\right)\frac{\gamma}{(\gamma-1)} + \frac{(1+\beta)}{2}\right](n+1)^3 \end{aligned} \tag{33}$$

In addition to the boundary conditions (33), the piston surface must also meet the requirement that the gas particles' speed be equal to the speed of the piston. The kinematic conditions of the piston surface can be expressed in a dimensionless form as:

$$V(y_p) = (n+1) \tag{34}$$

Additionally, The thermophysical parameter friction $\left(\tau = \mu\left(\frac{\partial V}{\partial y}\right)\right)$, rate of heat transfer $\left(Q^* = \int_{y_0}^{y_1}\frac{dQ}{dy}dy\right)$ and the total energy of the disturbance are calculated.

$$E_0 = 2\pi\lambda \int_{s_p}^{s_b} \rho \left[e + \frac{1}{2}v^2 + \frac{h}{\rho}\right] s^\lambda ds$$

Using the equation of state (6) and similarity transformations (21) in the above equation, we obtain:

$$E_0 = 2\pi\lambda\rho_a \left[\frac{CV_0}{(n+1){t_0}^n}\right]^{\frac{2}{(n+1)}} {s_b}^{(\lambda+3)-\frac{2}{(n+1)}} \times \int_{y_p}^{1} \left[\frac{P}{(\gamma-1)} + \frac{DV^2}{2} + A\right] y^{\lambda+2} dy \tag{35}$$

We note that the shock wave's total energy changes according to the radius of the shock wave, ${s_b}^{(\lambda+3)-\frac{2}{(n+1)}}$ and also pressure exerted by the internal expansion surface on the fluid can be used to increase the total amount of energy. In fact, shock waves in explosion situations are often complex and non-planar, making calculation of their total energy more difficult. Additionally, the presence of pre-existing defects or instabilities in the exploding material can affect the overall energy of the shock wave. Therefore, calculating the total energy of shock waves in explosion situations requires careful consideration of all the components involved. To obtain the numerical solution, it is reasonable to express the flow variables v, p, ρ, h and F in dimensionless form as follows:

$$\frac{v}{v_b} = \frac{V(y)}{V(1)}y, \quad \frac{p}{p_b} = \frac{P(y)}{P(1)}y^2, \quad \frac{\rho}{\rho_b} = \frac{D(y)}{D(1)}, \quad \frac{h}{h_b} = \frac{A(y)}{A(1)}y^2, \quad \frac{F}{F_b} = \frac{Q(y)}{Q(1)}y^3 \tag{36}$$

4. Results and Discussion

4.1. Numerical Study and Validation of Numerical Method

The mathematical computations are performed using MATLAB. Utilizing the fourth-order Runge-Kutta method, equations (28-32) were numerically integrated by incorporating the prescribed boundary conditions (33). It is feasible to approximate the distribution of flow variables between the shock front $(y = 1)$ and the inner expanding surface of the piston $(y = y_p)$. In this study, we consider the Cowling number range to be from 0 to 0.05, the Mach number to be from 1.2 to 5, the piston velocity index to be from -0.4 to -0.2, the Nusselt number to be from 0 to 385, and the coefficient of convective heat transfer to be from 0 to 10. These ranges were chosen with regard to relevant experimental or computational research in the literature, as well as conventional circumstances observed in shock wave processes. In the present investigation, it has been determined that the utilization of a uniform grid with a step size of $z^* = 0.0001$ demonstrates satisfactory convergence. The convergence criterion of 10^{-5} achieves an accuracy of 6 decimal places. Moreover, the solutions have been successfully obtained within a 10^{-6} tolerance error in all instances.

- **4-stage Runge-Kutta method**

In general, the system of five simultaneous non-linear ODEs with initial conditions is defined as follows:

$$\frac{dx_i}{dy} = f_i(y, V, D, A, P, Q), \quad x_i(y_0) = (x_i)_0, \quad i = 1,2,3,4,5 \tag{37}$$

Consider the 4-stage Runge-Kutta method for solving the system of five equations simultaneously:

where, $j_1 = k$, $j_2 = l$, $j_3 = m$, $j_4 = o$, $j_5 = n$, and $i = 1, 2, 3, 4, 5$,

$(j_i)_1 = z^* f_i(y, V, D, A, P, Q)$,

$(j_i)_2 = z^* f_i(y + c_2 z^*, V + a_{21}k_1, D + b_{21}l_1, A + d_{21}m_1, P + e_{21}o_1, Q + g_{21}n_1)$,

$(j_i)_3 = z^* f_i(y + c_3 z^*, V + a_{31}k_1 + a_{32}k_2, D + b_{31}l_1 + b_{32}l_2, A + d_{31}m_1 + d_{32}m_2, P + e_{31}o_1 + e_{32}o_2, Q + g_{31}n_1 + g_{32}n_2)$,

$(j_i)_4 = z^* f_i(y + c_4 z^*, V + a_{41}k_1 + a_{42}k_2 + a_{43}k_3, D + b_{41}l_1 + b_{42}l_2 + b_{43}l_3, A + d_{41}m_1 + d_{42}m_2 + d_{43}m_3, P + e_{41}o_1 + e_{42}o_2 + e_{43}o_3, Q + g_{41}n_1 + g_{42}n_2 + g_{43}n_3)$,

The solution of the system, (37) at $y = y_{n+1}$ is given by:

$(x_i)_{n+1} = (x_i)_n + \sum_{q=1}^{4} w_q (j_i)_q$, $i = 1, 2, 3, 4, 5$.

where the unknown coefficients a_{21}, b_{21}, d_{21}, e_{21}, g_{21}, a_{31}, a_{32}, b_{31}, b_{32}, d_{31}, d_{32}, e_{31}, e_{32}, g_{31}, g_{32}, a_{41}, a_{42}, a_{43}, b_{41}, b_{42}, b_{43}, d_{41}, d_{42}, d_{43}, e_{41}, e_{42}, e_{43}, g_{41}, g_{42}, g_{43}, c_2, c_3, c_4, and unknown weights w_1, w_2, w_3, w_4 have to be determined.

- **Stability**

Mathematically, a numerical method is said to be stable, if the effect of any single fixed round-off is bounded, independent of the number of mesh points [29].

For this current study, if for every $\varepsilon > 0$ there exists a $\delta = \delta(\varepsilon) > 0$, difference between two different numerical solutions $(x_i)_n$ and $\overline{(x_i)_n}$ such that

$\left|(x_i)_n - \overline{(x_i)_n}\right| < \varepsilon$, whenever $\left|(x_i)_0 - \overline{(x_i)_0}\right| < \delta(\varepsilon)$, $i = 1,2,3,4,5$.

We perform simulations with varied step sizes z^* to observe the solution's behaviour. It has been noticed that the solution does not increase substantially for varied values of z^*. It assures that the RK4 method is stable and produces trust worthy findings over lengthy interval. Therefore, the proposed fourth order RK method is stable.

- **Consistency**

The RK4 method's consistency demonstrates that the local truncation error vanishes as step size z^* approaches to zero [29]. We have by R-K method

$$(x_i)_{n+1} = (x_i)_n + \frac{1}{6}((j_i)_1 + 2(j_i)_2 + 2(j_i)_3 + (j_i)_4) \quad (38)$$

In this current study, for $i = 1, 2, 3, 4, 5$

$$(x_i)_{n+1} = (x_i)_n + z^*\varphi_i(y, V, D, A, P, Q, z^*), \quad n = 0,1,2,3 \ldots N-1 \quad (39)$$

where $\varphi(y, V, D, A, P, Q, z^*)$ is called increment function and $N = \frac{b-y_0}{z^*}$

The equation (39) is said to be consistent if

$$\varphi_i(y, V^*, D^*, A^*, P^*, Q^*, 0) = f_i(y, V, D, A, P, Q)$$

Substitute the $(j_i)_q$, $i = 1, 2, 3, 4, 5$, $q = 1,2,3,4$ values in the equation (38), we obtain

$$(x_i)_{n+1} = (x_i)_n + \frac{1}{6}\Big(z^* f_i(y, V, D, A, P, Q) + 2z^* f_i\left(y + \frac{z^*}{2}, V + \frac{k_1}{2}, D + \frac{l_1}{2}, A + \frac{m_1}{2}, P + \frac{o_1}{2}, Q + \frac{n_1}{2}\right) + 2z^* f_i\left(y + \frac{z^*}{2}, V + \frac{k_2}{2}, D + \frac{l_2}{2}, A + \frac{m_2}{2}, P + \frac{o_2}{2}, Q + \frac{n_2}{2}\right) + z^* f_i(y + h, V + k_3, D + l_3, A + m_3, P + o_3, Q + n_3)\Big), \quad (40)$$

$i = 1, 2, 3, 4, 5$

Comparing equations (40) and (39), we get

$$\varphi_i(y, V^*, D^*, A^*, P^*, Q^*, z^*) = \frac{1}{6}(f_i(y, V, D, A, P, Q)$$
$$+2f_i\left(y + \frac{z^*}{2}, V + \frac{k_1}{2}, D + \frac{l_1}{2}, A + \frac{m_1}{2}, P + \frac{o_1}{2}, Q + \frac{n_1}{2}\right)$$
$$+2f_i\left(y + \frac{z^*}{2}, V + \frac{k_2}{2}, D + \frac{l_2}{2}, A + \frac{m_2}{2}, P + \frac{o_2}{2}, Q + \frac{n_2}{2}\right)$$
$$+f_i(y + h, V + k_3, D + l_3, A + m_3, P + o_3, Q + n_3))$$

As $z^* \to 0$, we get

$$\varphi_i(y, V^*, D^*, A^*, P^*, Q^*, 0) = \frac{(1 + 2 + 2 + 1)}{6} f_i(y, V, D, A, P, Q) = f_i(y, V, D, A, P, Q)$$

Therefore, the proposed fourth order RK method is consistent.

- **Regularity**

It ensures that the approach does not fail due to discontinuities or abnormalities in the system of equations [29].

here, mathematically, For $i = 1, 2, 3, 4, 5$

$$(x_i)_{n+1} = (x_i)_n + z^*\varphi_i(y, V, D, A, P, Q, z^*), \quad n = 0,1,2,3 \ldots, N-1$$

A method is said to be regular, if the function $\varphi_i(y, V, D, A, P, Q, z^*)$ is defined and continuous in the domain $y_0 \le y \le b$ and $y, V, D, A, P, Q \in \mathrm{R}$, $z^* \in [0, {z_0}^*]$ (${z_0}^*$ is a positive constant) and if there exists a constant $L > 0$ such that:

$$|\varphi(y, V, D, A, P, Q, z^*) - \varphi(y, V^*, D^*, A^*, P^*, Q^*, z^*)| \le L(|V - V^*| + |D - D^*| + |A - A^*| + |P - P^*| + |Q - Q^*|)$$

That is, if the increment function (mentioned in equation 39) satisfies the Lipschitz condition, then the proposed fourth order RK method is regular.

$$|\varphi_i(y, V, D, A, P, Q, z^*) - \varphi_i(y, V^*, D^*, A^*, P^*, Q^*, z^*)| = {z^*}^{-1}\left|\sum_{q=1}^{4} w_q (j_i)_q - \sum_{q=1}^{4} w_q {(j_i)^*}_q\right|, \quad (41)$$

$i = 1, 2, 3, 4, 5$

We know that $f_i(y, V, D, A, P, Q)$ satisfies the Lipschitz condition. Thus $(j_i)_q$, $i = 1, 2, 3, 4, 5$, $q = 1,2,3,4$ satisfy the following relations.

$$(j_i)_1 = z^* f_i(y, V, D, A, P, Q)$$
$$\left|(j_i)_1 - {(j_i)^*}_1\right| = |z^* f_i(y, V, D, A, P, Q) - z^* f_i(y, V^*, D^*, A^*, P^*, Q^*)| \quad (42)$$
$$\le z^* L(|V - V^*| + |D - D^*| + |A - A^*| + |P - P^*| + |Q - Q^*|)$$

$$(j_i)_2 = z^* f_i(y + c_2 z^*, V + a_{21}k_1, D + b_{21}l_1, A + d_{21}m_1, P + e_{21}o_1, Q + g_{21}n_1)$$

$$\left|(j_i)_2 - (j_i)^*{}_2\right| = |z^* f_i(y + c_2 z^*, V + a_{21}k_1, D + b_{21}l_1, A + d_{21}m_1, P + e_{21}o_1, Q + g_{21}n_1) - z^* f_i(y + c_2 z^*, V^* + a_{21}k_1{}^*, D^* + b_{21}l_1{}^*, A^* + d_{21}m_1{}^*, P^* + e_{21}o_1{}^*, Q^* + g_{21}n_1{}^*)|$$

$$\leq z^* L(|V + a_{21}k_1 - (V^* + a_{21}k_1{}^*)| + |D + b_{21}l_1 - (D^* + b_{21}l_1{}^*)| + |A + d_{21}m_1 - (A^* + d_{21}m_1{}^*)| + |P + e_{21}o_1 - (P^* + e_{21}o_1{}^*)| + |Q + g_{21}n_1 - (Q^* + g_{21}n_1{}^*)|)$$

$$\left|(j_i)_2 - (j_i)^*{}_2\right| \leq z^* L(|(V - V^*) + a_{21}(k_1 - k_1{}^*)| + |(D - D^*) + b_{21}(l_1 - l_1{}^*)| + |(A - A^*) + d_{21}(m_1 - m_1{}^*)| + |(P - P^*) + e_{21}(o_1 - o_1{}^*)| + |(Q - Q^*) + g_{21}(n_1 - n_1{}^*)|)$$

Substitute the $\left|(j_i)_1 - (j_i)^*{}_1\right|, i = 1, 2, 3, 4, 5,$ values in the above equation (42). Then we obtain:

$$\left|(j_i)_2 - (j_i)^*{}_2\right| \leq z^* L\big((|V - V^*| + |D - D^*| + |A - A^*| + |P - P^*| + |Q - Q^*|) \times (1 + z^* L a_{21} + z^* L b_{21} + z^* L d_{21} + z^* L e_{21} + z^* L g_{21})$$

$$(j_i)_3 = z^* f_i(y + c_3 z^*, V + a_{31}k_1 + a_{32}k_2, D + b_{31}l_1 + b_{32}l_2, A + d_{31}m_1 + d_{32}m_2, P + e_{31}o_1 + e_{32}o_2, Q + g_{31}n_1 + g_{32}n_2)$$

$$\begin{aligned}\left|(j_i)_3 - (j_i)^*{}_3\right| \leq\ & |z^* f_i(y + c_3 z^*, V + a_{31}k_1 + a_{32}k_2, D + b_{31}l_1 + b_{32}l_2, A + d_{31}m_1 + d_{32}m_2, P + e_{31}o_1 + e_{32}o_2, Q + g_{31}n_1 + g_{32}n_2) \\ & - z^* f_i(y + c_3 z^*, V^* + a_{31}k_1{}^* + a_{32}k_2{}^*, D^* + b_{31}l_1{}^* + b_{32}l_2{}^*, A^* + d_{31}m_1{}^* + d_{32}m_2{}^*, P^* + e_{31}o_1{}^* + e_{32}o_2{}^*, Q^* + g_{31}n_1{}^* + g_{32}n_2{}^*)| \\ & \leq z^* L(|V + a_{31}k_1 + a_{32}k_2 - (V^* + a_{31}k_1{}^* + a_{32}k_2{}^*)| \\ & + |D + b_{31}l_1 + b_{32}l_2 - (D^* + b_{31}l_1{}^* + b_{32}l_2{}^*)| \\ & + |A + d_{31}m_1 + d_{32}m_2 - (A^* + d_{31}m_1{}^* + d_{32}m_2{}^*)| \\ & + |P + e_{31}o_1 + e_{32}o_2 - (P^* + e_{31}o_1{}^* + e_{32}o_2{}^*)| \\ & + |Q + g_{31}n_1 + g_{32}n_2 - (Q^* + g_{31}n_1{}^* + g_{32}n_2{}^*)|)\end{aligned} \tag{43}$$

$$\begin{aligned}\left|(j_i)_3 - (j_i)^*{}_3\right| \leq\ & z^* L(|(V - V^*) + a_{31}(k_1 - k_1{}^*) + a_{32}(k_2 - k_2{}^*)| + |(D - D^*) + b_{31}(l_1 - l_1{}^*) \\ & + b_{32}(l_2 - l_2{}^*)| + |(A - A^*) + d_{31}(m_1 - m_1{}^*) + d_{32}(m_2 - m_2{}^*)| \\ & + |(P - P^*) + e_{31}(o_1 - o_1{}^*) + e_{32}(o_2 - o_2{}^*)| \\ & + |(Q - Q^*) + g_{31}(n_1 - n_1{}^*) + g_{32}(n_2 - n_2{}^*)|)\end{aligned}$$

Substitute the $\left|(j_i)_1 - (j_i)^*{}_1\right|$, $\left|(j_i)_2 - (j_i)^*{}_2\right|$, $i = 1, 2, 3, 4, 5,$ values in the above equation (43). We obtain:

$$\begin{aligned}\left|(j_i)_3 - (j_i)^*{}_3\right| \leq\ & z^* L(|V - V^*| + |D - D^*| + |A - A^*| + |P - P^*| + |Q - Q^*|) \\ & \times (1 + z^* L a_{31} + z^* L a_{32}(1 + z^* L a_{21} + z^* L b_{21} + z^* L d_{21} + z^* L e_{21} + z^* L g_{21}) \\ & + z^* L b_{31} + z^* L b_{32}(1 + z^* L a_{21} + z^* L b_{21} + z^* L d_{21} + z^* L e_{21} + z^* L g_{21}) \\ & + z^* L d_{31} + z^* L d_{32}(1 + z^* L a_{21} + z^* L b_{21} + z^* L d_{21} + z^* L e_{21} + z^* L g_{21}) \\ & + z^* L e_{31} + z^* L e_{32}(1 + z^* L a_{21} + z^* L b_{21} + z^* L d_{21} + z^* L e_{21} + z^* L g_{21}) \\ & + z^* L g_{31} + z^* L g_{32}(1 + z^* L a_{21} + z^* L b_{21} + z^* L d_{21} + z^* L e_{21} + z^* L g_{21})\big)\end{aligned} \tag{44}$$

$$\begin{aligned}\left|(j_i)_4 - (j_i)^*{}_4\right| \leq\ & |z^* f_i(y + z^*, V + k_3, D + l_3, A + m_3, P + o_3, Q + n_3) \\ & - z^* f_i(y + z^*, V^* + k_3{}^*, D^* + l_3{}^*, A^* + m_3{}^*, P^* + o_3{}^*, Q^* + n_3{}^*)| \\ & \leq z^* L(|V - V^*| + |D - D^*| + |A - A^*| + |P - P^*| + |Q - Q^*|) \times \\ & (1 + z^* L a_{41} + z^* L a_{42}(1 + z^* L a_{21} + z^* L b_{21} + z^* L d_{21} + z^* L e_{21} + z^* L g_{21}) + \\ & z^* L a_{43}(1 + z^* L a_{31} + z^* L a_{32}(1 + z^* L a_{21} + z^* L b_{21} + z^* L d_{21} + z^* L e_{21} + z^* L g_{21}) +\end{aligned}$$

$$z^*Lb_{31} + z^*Lb_{32}(1 + z^*La_{21} + z^*Lb_{21} + z^*Ld_{21} + z^*Le_{21} + z^*Lg_{21}) +$$
$$z^*Ld_{31} + z^*Ld_{32}(1 + z^*La_{21} + z^*Lb_{21} + z^*Ld_{21} + z^*Le_{21} + z^*Lg_{21}) +$$
$$z^*Le_{31} + z^*Le_{32}(1 + z^*La_{21} + z^*Lb_{21} + z^*Ld_{21} + z^*Le_{21} + z^*Lg_{21}) +$$
$$z^*Lg_{31} + z^*Lg_{32}(1 + z^*La_{21} + z^*Lb_{21} + z^*Ld_{21} + z^*Le_{21} + z^*Lg_{21})\big) +$$
$$(z^*Lb_{41} + z^*Lb_{42}(1 + z^*La_{21} + z^*Lb_{21} + z^*Ld_{21} + z^*Le_{21} + z^*Lg_{21}) +$$
$$z^*Lb_{43}(1 + z^*La_{31} + z^*La_{32}(1 + z^*La_{21} + z^*Lb_{21} + z^*Ld_{21} + z^*Le_{21} + z^*Lg_{21}) +$$
$$z^*Lb_{31} + z^*Lb_{32}(1 + z^*La_{21} + z^*Lb_{21} + z^*Ld_{21} + z^*Le_{21} + z^*Lg_{21}) +$$
$$z^*Ld_{31} + z^*Ld_{32}(1 + z^*La_{21} + z^*Lb_{21} + z^*Ld_{21} + z^*Le_{21} + z^*Lg_{21}) +$$
$$z^*Le_{31} + z^*Le_{32}(1 + z^*La_{21} + z^*Lb_{21} + z^*Ld_{21} + z^*Le_{21} + z^*Lg_{21}) +$$
$$z^*Lg_{31} + z^*Lg_{32}(1 + z^*La_{21} + z^*Lb_{21} + z^*Ld_{21} + z^*Le_{21} + z^*Lg_{21})\big) +$$
$$(z^*Ld_{41} + z^*Ld_{42}(1 + z^*La_{21} + z^*Lb_{21} + z^*Ld_{21} + z^*Le_{21} + z^*Lg_{21}) +$$
$$z^*Ld_{43}(1 + z^*La_{31} + z^*La_{32}(1 + z^*La_{21} + z^*Lb_{21} + z^*Ld_{21} + z^*Le_{21} + z^*Lg_{21}) +$$
$$z^*Lb_{31} + z^*Lb_{32}(1 + z^*La_{21} + z^*Lb_{21} + z^*Ld_{21} + z^*Le_{21} + z^*Lg_{21}) +$$
$$z^*Ld_{31} + z^*Ld_{32}(1 + z^*La_{21} + z^*Lb_{21} + z^*Ld_{21} + z^*Le_{21} + z^*Lg_{21}) +$$
$$z^*Le_{31} + z^*Le_{32}(1 + z^*La_{21} + z^*Lb_{21} + z^*Ld_{21} + z^*Le_{21} + z^*Lg_{21}) +$$
$$z^*Lg_{31} + z^*Lg_{32}(1 + z^*La_{21} + z^*Lb_{21} + z^*Ld_{21} + z^*Le_{21} + z^*Lg_{21})\big) +$$
$$(z^*Le_{41} + z^*Le_{42}(1 + z^*La_{21} + z^*Lb_{21} + z^*Ld_{21} + z^*Le_{21} + z^*Lg_{21}) +$$
$$z^*Le_{43}(1 + z^*La_{31} + z^*La_{32}(1 + z^*La_{21} + z^*Lb_{21} + z^*Ld_{21} + z^*Le_{21} + z^*Lg_{21}) +$$
$$z^*Lb_{31} + z^*Lb_{32}(1 + z^*La_{21} + z^*Lb_{21} + z^*Ld_{21} + z^*Le_{21} + z^*Lg_{21}) +$$
$$z^*Ld_{31} + z^*Ld_{32}(1 + z^*La_{21} + z^*Lb_{21} + z^*Ld_{21} + z^*Le_{21} + z^*Lg_{21}) +$$
$$z^*Le_{31} + z^*Le_{32}(1 + z^*La_{21} + z^*Lb_{21} + z^*Ld_{21} + z^*Le_{21} + z^*Lg_{21}) +$$
$$z^*Lg_{31} + z^*Lg_{32}(1 + z^*La_{21} + z^*Lb_{21} + z^*Ld_{21} + z^*Le_{21} + z^*Lg_{21})\big) +$$
$$(z^*Lg_{41} + z^*Lg_{42}(1 + z^*La_{21} + z^*Lb_{21} + z^*Ld_{21} + z^*Le_{21} + z^*Lg_{21}) +$$
$$z^*Lg_{43}(1 + z^*La_{31} + z^*La_{32}(1 + z^*La_{21} + z^*Lb_{21} + z^*Ld_{21} + z^*Le_{21} + z^*Lg_{21}) +$$
$$z^*Lb_{31} + z^*Lb_{32}(1 + z^*La_{21} + z^*Lb_{21} + z^*Ld_{21} + z^*Le_{21} + z^*Lg_{21}) +$$
$$z^*Ld_{31} + z^*Ld_{32}(1 + z^*La_{21} + z^*Lb_{21} + z^*Ld_{21} + z^*Le_{21} + z^*Lg_{21}) +$$
$$z^*Le_{31} + z^*Le_{32}(1 + z^*La_{21} + z^*Lb_{21} + z^*Ld_{21} + z^*Le_{21} + z^*Lg_{21}) +$$
$$z^*Lg_{31} + z^*Lg_{32}(1 + z^*La_{21} + z^*Lb_{21} + z^*Ld_{21} + z^*Le_{21} + z^*Lg_{21})\big)\Big)$$

From the equation (41) implies that for $i = 1, 2, 3, 4, 5$

$$\begin{aligned}&|\varphi_i(y, V, D, A, P, Q, z^*) - \varphi_i(y, V^*, D^*, A^*, P^*, Q^*, z^*)| = {z^*}^{-1}\left|\sum_{q=1}^{4} w_q (j_i)_q - \sum_{q=1}^{4} w_q {(j_i)^*}_q\right| = \\ &{z^*}^{-1}\left|w_1(j_i)_1 + w_2(j_i)_2 + w_3(j_i)_3 + w_4(j_i)_4 - w_1{(j_i)^*}_1 + w_2{(j_i)^*}_2 + w_3{(j_i)^*}_3 + w_4{(j_i)^*}_4\right| \\ &|\varphi_i(y, V, D, A, P, Q, z^*) - \varphi_i(y, V^*, D^*, A^*, P^*, Q^*, z^*)| \\ &\leq {z^*}^{-1}\left(w_1\left|(j_i)_1 - {(j_i)^*}_1\right| + w_2\left|(j_i)_2 - {(j_i)^*}_2\right| + w_3\left|(j_i)_3 - {(j_i)^*}_3\right| + w_4\left|(j_i)_4 - {(j_i)^*}_4\right|\right)\end{aligned} \tag{45}$$

Substitute the $\left|(j_i)_1 - {(j_i)^*}_1\right|$, $\left|(j_i)_2 - {(j_i)^*}_2\right|$, $\left|(j_i)_3 - {(j_i)^*}_3\right|$, $\left|(j_i)_4 - {(j_i)^*}_4\right|$ $i = 1, 2, 3, 4, 5,$ values in the above equation (45) to obtain:

$$\begin{aligned}&\leq L(|V - V^*| + |D - D^*| + |A - A^*| + |P - P^*| + |Q - Q^*|)(w_1 + w_2 + w_3 + w_4) + \\ &\big(w_2(a_{21} + b_{21} + d_{21} + e_{21} + g_{21}) + w_3\big((a_{31} + a_{32}) + (b_{31} + b_{32}) + (d_{31} + d_{32}) + \\ &(e_{31} + e_{32}) + (g_{31} + g_{32})\big) + w_4\big((a_{41} + a_{42} + a_{43}) + (b_{41} + b_{42} + b_{43}) + \\ &(d_{41} + d_{42} + d_{43}) + (e_{41} + e_{42} + e_{43}) + (g_{41} + g_{42} + g_{43})\big)\big)(z^*L) +\end{aligned} \tag{46}$$

$$w_3 a_{32}(a_{21}+b_{21}+d_{21}+e_{21}+g_{21}) + w_3 b_{32}(a_{21}+b_{21}+d_{21}+e_{21}+g_{21}) +$$
$$w_3 d_{32}(a_{21}+b_{21}+d_{21}+e_{21}+g_{21}) + w_3 e_{32}(a_{21}+b_{21}+d_{21}+e_{21}+g_{21}) +$$
$$w_3 g_{32}(a_{21}+b_{21}+d_{21}+e_{21}+g_{21}) + w_4 a_{42}(a_{21}+b_{21}+d_{21}+e_{21}+g_{21}) +$$
$$w_4 b_{42}(a_{21}+b_{21}+d_{21}+e_{21}+g_{21}) + w_4 d_{42}(a_{21}+b_{21}+d_{21}+e_{21}+g_{21}) +$$
$$w_4 e_{42}(a_{21}+b_{21}+d_{21}+e_{21}+g_{21}) + w_4 g_{42}(a_{21}+b_{21}+d_{21}+e_{21}+g_{21}) +$$
$$w_4 a_{43}\big((a_{31}+a_{32})+(b_{31}+b_{32})+(d_{31}+d_{32})+(e_{31}+e_{32})+(g_{31}+g_{32})\big) +$$
$$w_4 b_{43}\big((a_{31}+a_{32})+(b_{31}+b_{32})+(d_{31}+d_{32})+(e_{31}+e_{32})+(g_{31}+g_{32})\big) +$$
$$w_4 d_{43}\big((a_{31}+a_{32})+(b_{31}+b_{32})+(d_{31}+d_{32})+(e_{31}+e_{32})+(g_{31}+g_{32})\big) +$$
$$w_4 e_{43}\big((a_{31}+a_{32})+(b_{31}+b_{32})+(d_{31}+d_{32})+(e_{31}+e_{32})+(g_{31}+g_{32})\big) +$$
$$w_4 g_{43}\big((a_{31}+a_{32})+(b_{31}+b_{32})+(d_{31}+d_{32})+(e_{31}+e_{32})+(g_{31}+g_{32})\big) \times$$
$$(z^*L)^2 + (w_4 a_{43} a_{32}(a_{21}+b_{21}+d_{21}+e_{21}+g_{21}) +$$
$$w_4 b_{43} b_{32}(a_{21}+b_{21}+d_{21}+e_{21}+g_{21}) +$$
$$w_4 d_{43} d_{32}(a_{21}+b_{21}+d_{21}+e_{21}+g_{21}) +$$
$$w_4 e_{43} e_{32}(a_{21}+b_{21}+d_{21}+e_{21}+g_{21}) +$$
$$w_4 g_{43} g_{32}(a_{21}+b_{21}+d_{21}+e_{21}+g_{21}))(z^*L)^3$$
$$\leq L(|V-V^*|+|D-D^*|+|A-A^*|+|P-P^*|+|Q-Q^*|)\left(1+\frac{5}{2}z^*L+\frac{25}{6}(z^*L)^2+\frac{25}{24}(z^*L)^3\right)$$

So, the proposed method of RK4 is regular.

- **Convergence Analysis**

Theorem: A necessary and sufficient condition for convergence of a regular single-step method of order $p \geq 1$ is consistency [29, 30]

Convergence refers to the method's capacity to produce an approximation solution that becomes closer to the exact solution as the step size reduces [29]. Mathematically, for this current study, a numerical method is said to be convergent if $\lim_{n\to\infty}(x_i)_n = x_i(y_n)$, for all $y_n \in [y_0, b]$, $y_n = y_0 + nz^*$

In the equation (39), the true value of $x_i(y_{n+1})$ is given by

$x_i(y_{n+1}) = x_i(y_n) + z^*\varphi_i(y, V, D, A, P, Q, z^*) + T_n$, $n = 0,1,2,3 \dots, N-1$, $i = 1, 2, 3, 4, 5$, here T_n is truncation error.

It directly connects local truncation errors to global errors across the entire solution. By evaluating convergence, we ensure that the RK4 method's errors diminish as the step size decreases, resulting in an accurate method for solving the system of equations.

Since the RK4 method meets all four criteria (stability, consistency, regularity, and convergence), we can conclude that it is mathematically valid for solving the given system of equations. It ensures reliable local approximation of the differential equations and can handle the smoothness of the solutions. As a result, the method will produce accurate numerical solutions for sufficiently small step size and well- behaved problems, yielding consistent results over the whole domain of the similarity variable y.

4.2. Observations and Findings

This section examines how flow variables like velocity, density, pressure, magnetic pressure, and energy behave under different piston velocity index n in order to investigate the physical effects of convective heat transfer and magnetic field on shock wave propagation in spherical and cylindrical geometries.

- *Analysis of the presence of convective heat transfer on flow variables in the absence of a magnetic field:*

In consideration of convective heat transfer, the variations in flow variables (pressure and energy) are more, whereas they are less in the case of velocity and density profiles (see Figs. 2(a, f), 2(b, g), 2(c, h), 2(e, j)) for spherical geometry and variations in velocity, density, and energy are greater, whereas they are less in the case of pressure in cylindrical geometry (see Figs. 3(a, f), 3(b, g), 3(c, h), 3(e, j)). A reversed behavior of the flow variables (v/v_b, ρ/ρ_b, p/p_b, F/F_b) is obtained for $n = -0.3$, -0.4 in the presence of convection (see Figs. 2(a, f), 2(b, g), 2(c, h), and 2(e, j)) in spherical geometry. This suggests a nonlinear relationship between the convection-induced thermal boundary layer and the piston velocity index. The thermal convection dominates over the piston velocity index, leading to rarefaction in density and pressure fields and backward heat transfer. But there is no reverse behaviour in the case of cylindrical geometry. The interaction between shock dynamics and heat transfer is critically influenced by geometry. Smoother transition and suppression of reversed trends result of axial redistribution of heat and momentum supported by the cylindrical structure. The effects of convection alter the velocity, density, pressure, and energy distribution of the shock wave, potentially leading to different behavior for different piston velocities. This type of alternating behavior of convective heat transfer exists in the literature [26].

- *Analysis of the influence of magnetic field on flow variables in the absence of convective heat transfer:*

It is worth noting that, in both spherical and cylindrical cases, the flow parameters v/v_b and F/F_b (as shown in Fig. 2 (a, e)) have low values at the shock front and increase more rapidly over the interval of y from the shock front for fixed values of the piston velocity index n. This is because the shock waves become more intense with time, which causes the piston to travel faster than the velocities of the gas particles in the fluid behind the shock front. Due to the magnetic resistance (Lorentz force) created by the magnetic field, fluid motion is opposed, resulting in decreased energy and velocity close to the shock front. It is observed that, in spherical geometry, in the presence of a magnetic field, this behavior diminishes for energy distribution and increases for velocity distribution as the piston velocity index n increases, but for cylindrical geometry, this behavior diminishes for both energy and velocity distribution. In the absence of a magnetic field, these flow variables exhibit similar behavior. It is noteworthy that in the presence of a magnetic field, the velocity and energy profile rapidly fall after the shock front. This is due to the increase in the Cowling number C_a, which causes a decrease in y_p (indicating a reduction in piston velocity v_p) (see Table 1). Additionally, as the disturbed area between the shock and piston widens, magnetic flux compression occurs, which in turn lowers the magnetic field h/h_b (see Fig. 2(d)).

In the spherical geometry, it is observed that the pressure (p/p_b) increases suddenly and reaches a high peak near the shock front. However, it then decreases rapidly at a certain distance (interval of y) from the shock front and increases again at a point in the flow field behind the shock front, with increasing values of the piston velocity index n, in the absence of a magnetic field. It is very interesting to note that this sudden peak near the shock front in the pressure profiles (p/p_b) (see Fig. 2(c)) disappears under the influence of a magnetic field, indicating shock weakening with stronger magnetic field effects. Moreover, it decreases gradually and eventually vanishes at a certain distance (interval of y) from the shock front, creating a perfect vacuum. The prerequisites for creating a shock wave in a lab environment are satisfied. Furthermore, it has been noted that the pressure decreases gradually as the piston velocity index n increases. Fig. 2(d) shows that the magnetic pressure profiles have a smooth, gradual decrease (which is almost insignificant) at a certain distance (interval of y) near the shock front. These profiles originate from the same value at the shock front ($y = 1$) for different values of the piston velocity index n. It is also observed that in spherical geometry, a discontinuity appears in the magnetic pressure (h/h_b) profiles near the shock front and then reduces quickly and eventually vanishes at a certain distance (interval of y) from the shock front. This is due to magnetic flux compression. Furthermore, it has been noted that the magnetic pressure profiles decrease gradually with increasing values in the piston velocity index n. Density (ρ/ρ_b) increases gradually behind the shock front in the presence of a magnetic field, and this increase is further amplified with an increase in the piston velocity index n (see Fig. 2(b)). This can be attributed to the fact that the concentration of gas particles is higher near the piston compared to the mass concentration at the shock front. From a physical perspective, this means that when a shock wave travels perpendicular to a magnetic field, the wave's compression of gas particles causes the field strength to increase, which is directly correlated with the gas density. Related studies on real-life applications of heat transfer in a MHD regime are reported in the literature [27, 38]. But compared to the spherical case, pressure distribution is high in the case of cylindrical geometry (see. Fig. 2(c), 2(h), 3(c) and 3(h)). From 3(c) and 3(h) we can observe that, sudden peaks near the shock front in the pressure profile are not present but similar to spherical geometry, a perfect vacuum is created. The prerequisites for creating a shock wave in a lab environment are satisfied. It is also observed that, for cylindrical geometry, magnetic pressure (h/h_b) profiles (see 3(d)) near the shock front exhibit fluctuations, but eventually they decay rapidly. But a sudden rise in the h/h_b profile for $n = -0.4$ is explicitly visible. This indicates that cylindrical symmetry results in prolonged magnetic compression in the front region, leading to sustained magnetic compression.

- *Analysis of the combined effect of convection and magnetic field:*

It can be observed for the spherical geometry case from Figs. 2(b, g) that the flow variable profiles for $n = -0.4$ exhibit a quicker decay, while p/p_b and h/h_b (as shown in Figs. 2(c, h) and 2(d, i)) experience faster growth compared to the case where only the magnetic field is considered. This is because heat transfer increases compressibility, which leads to increased pressure amplification, while convection lowers post-shock density, allowing the magnetic pressure gradient to steepen.

Fig. 2(g) shows that, for fixed values of the piston velocity index n, the density distribution reduces at every point in the interval of y from the shock front. It is evident from equation (28) that there is a singularity at the piston surface when the kinematic condition (33) holds. For piston velocities associated with (curves 1-5 in Fig. 2(g)), these singularities can be removed, and a finite solution for $D(y)$ is obtained. Curve 6 in Fig. 2(g) shows a non-removable singularity where the derivative of density tends to negative infinity. This singularity can be explained by the density ρ/ρ_b (see density variation curve for $n = -0.4$), where the path of the decelerating piston deviates from the path of gas particles immediately ahead of the shock front, resulting in a rarefaction of the gas. This results in a sudden drop in density near the piston, causing the temperature to approach zero or infinity. Shock wave instability caused by convection and deceleration working together is indicated by this singularity. Similar trends in flow variables for heat transfer in the presence of magnetic fields are reported by [24].

It is evident from Figure 3(b) and 3(g), that, for $n = -0.4$, the density profile has a sudden pit, in the absence of convection, that completely disappears in the presence of convection, confirming its stabilizing thermal effect. There is a reverse behavior of the velocity profile observed, but for other flow variables there is no reversed behavior observed.

Compared to the profiles (density, pressure, magnetic pressure, and energy) in the absence of convection, the values of p/p_b and h/h_b are decreasing and ρ/ρ_b and F/F_b are increasing in the presence of convection. Convection suppresses steep gradients in the cylindrical geometry resulting in flows that are smoother but energetically rich flows.

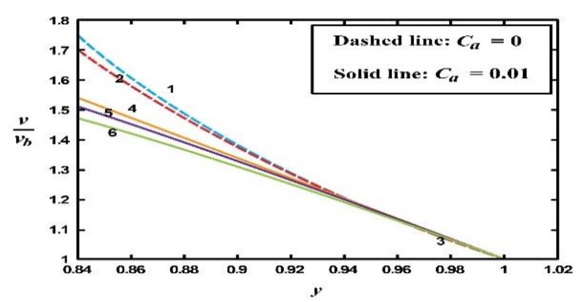

(a) Velocity profiles for $\Gamma_{Cn} = 0$

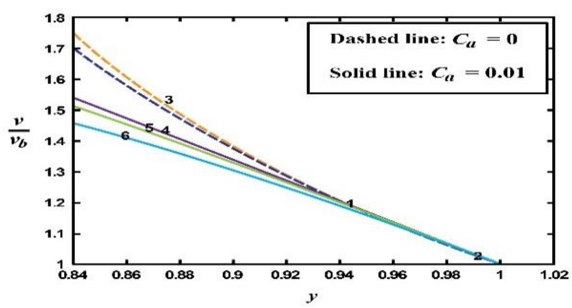

(f) Velocity profiles for $\Gamma_{Cn} = 10$

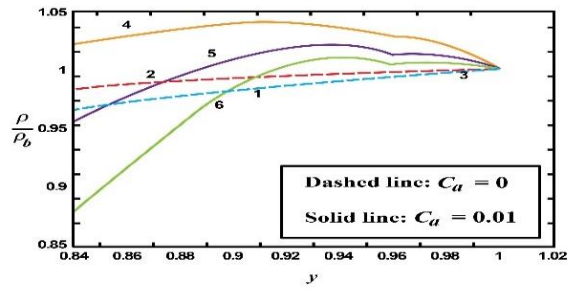

(b) Density profiles for $\Gamma_{Cn} = 0$

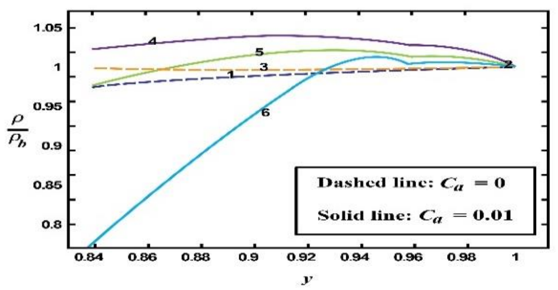

(g) Density profiles for $\Gamma_{Cn} = 10$

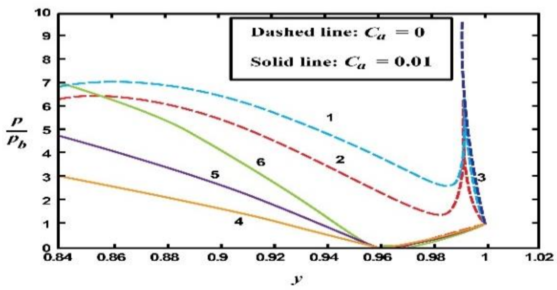

(c) Pressure profiles for $\Gamma_{Cn} = 0$

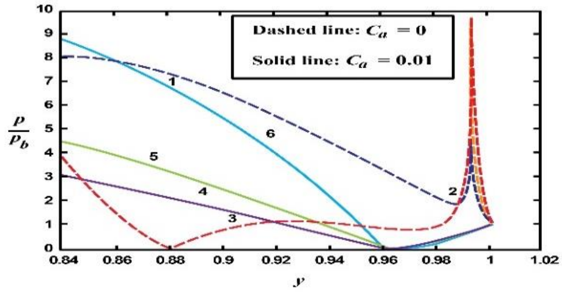

(h) Pressure profiles for $\Gamma_{Cn} = 10$

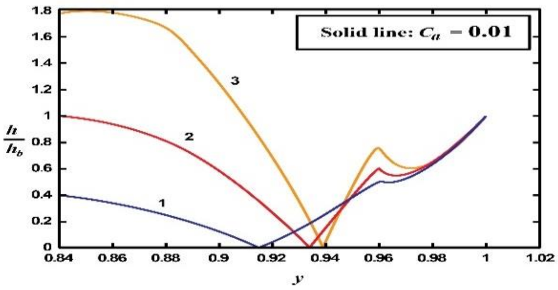

(d) Magnetic Pressure profiles for $\Gamma_{Cn} = 0$

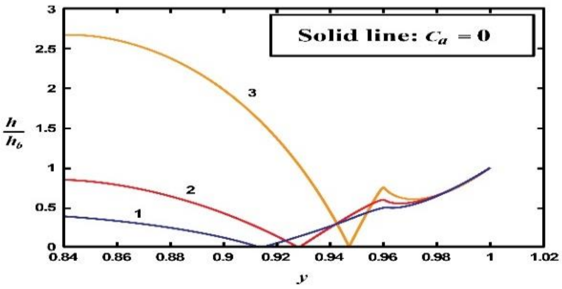

(i) Magnetic Pressure profiles for $\Gamma_{Cn} = 10$

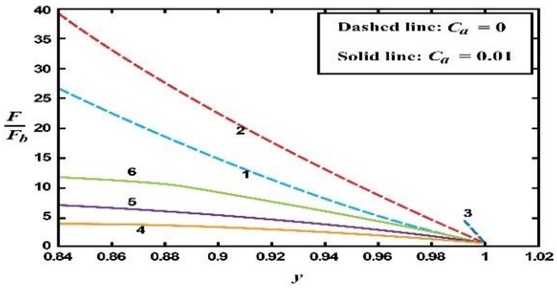

(e) Energy profiles for $\Gamma_{Cn} = 0$

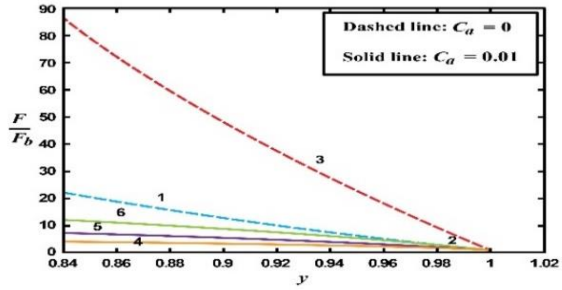

(j) Energy profiles for $\Gamma_{Cn} = 10$

Fig. 2. Changes in the lowered flow parameters in the area behind the shock front with $\gamma = 5/3$, $\Gamma_{Cd} = 10$, $\Gamma_{Rd} = 10$, $\delta_c = \beta = m = \eta = 1$, $\delta_R = \lambda = 2$, $M = 5$, *(a, f)* fluid velocity $\frac{v}{v_b}$, *(b, g)* density $\frac{\rho}{\rho_b}$, *(c, h)* pressure $\frac{p}{p_b}$, *(d, i)* magnetic pressure $\frac{h}{h_b}$, *(e, j)* energy $\frac{F}{F_b}$; ($C_a = 0$ (1)$n = -0.2$, (2)$n = -0.3$, (3)$n = -0.4$), ($C_a = 0.01$ (4)$n = -0.2$, (5) $n = -0.3$, (6) $n = -0.4$)) for spherical geometry

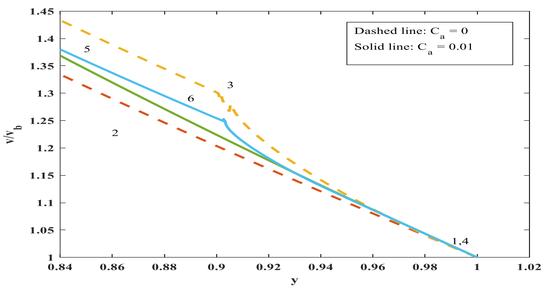

(a) Velocity profiles for $\Gamma_{Cn} = 0$

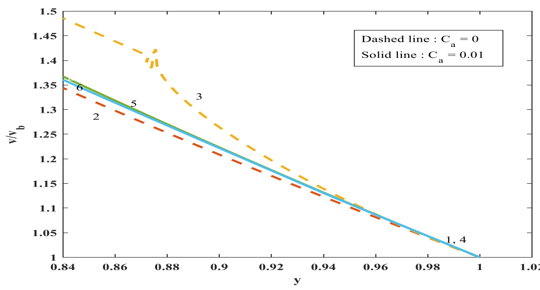

(f) Velocity profiles for $\Gamma_{Cn} = 10$

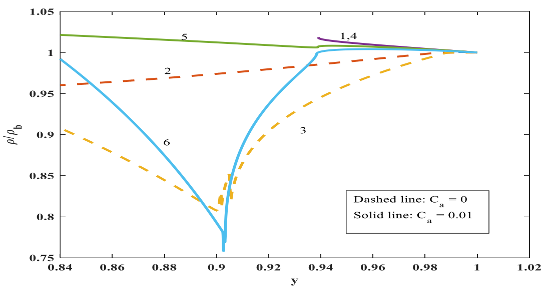

(b) Density profiles for $\Gamma_{Cn} = 0$

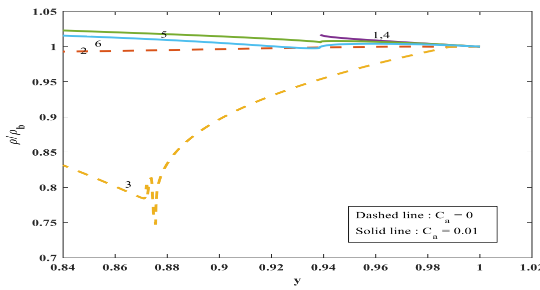

(g) Density profiles for $\Gamma_{Cn} = 10$

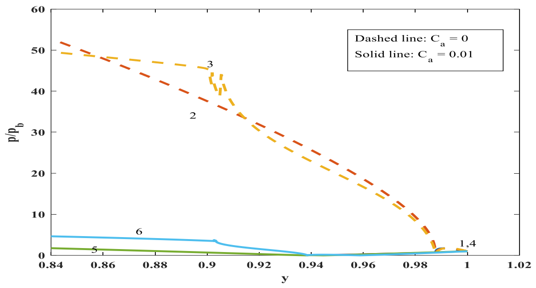

(c) Pressure profiles for $\Gamma_{Cn} = 0$

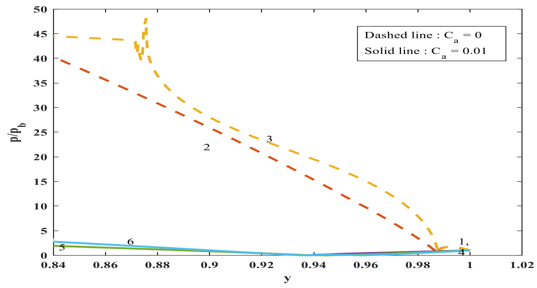

(h) Pressure profiles for $\Gamma_{Cn} = 10$

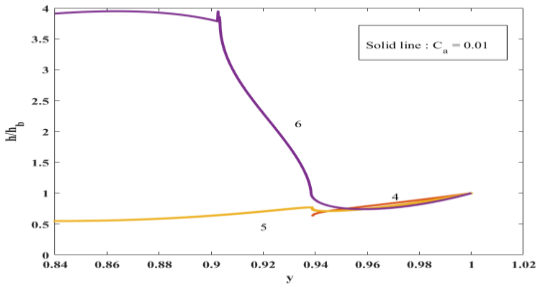

(d) Magnetic Pressure profiles for $\Gamma_{Cn} = 0$

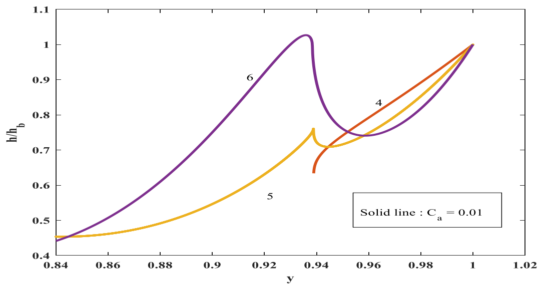

(i) Magnetic Pressure profiles for $\Gamma_{Cn} = 10$

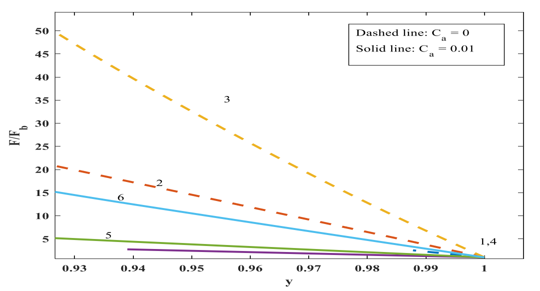

(e) Energy profiles for $\Gamma_{Cn} = 0$

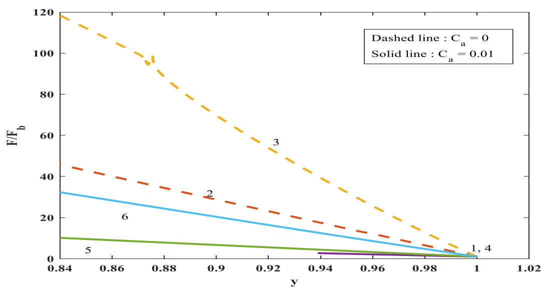

(j) Energy profiles for $\Gamma_{Cn} = 10$

Fig. 3. Changes in the lowered flow parameters in the area behind the shock front with $\gamma = 5/3, \Gamma_{Cd} = 10, \Gamma_{Rd} = 10, \delta_c = \beta = m = \eta = \lambda = 1, \delta_R = 2, M = 5$, *(a, f)* fluid velocity $\frac{v}{v_b}$, *(b, g)* density $\frac{\rho}{\rho_b}$, *(c, h)* pressure $\frac{p}{p_b}$, *(d, i)* magnetic pressure $\frac{h}{h_b}$, *(e, j)* energy $\frac{F}{F_b}$; ($C_a = 0$ (1)$n = -0.2$, (2)$n = -0.3$, (3)$n = -0.4$), ($C_a = 0.01$ (4)$n = -0.2$, (5) $n = -0.3$, (6) $n = -0.4$)) for cylindrical geometry

Table 1. The location of the inner boundary surface y_p for different values of Cowling number C_a with respect to the density ratio β (ρ/ρ_b) across the shock with $\gamma = 5/3$, $\delta_c = \beta = m = \eta = 1, \delta_R = 2, \Gamma_{cd} = 10, \Gamma_{Rd} = 10, M = 5$

C_a	β	$1-\beta$	y_p
0	0.0240	0.976	0.9766
0.01	0.1184	0.8816	0.8941
0.02	0.1651	0.8349	0.8583
0.05	0.2636	0.7364	0.7913

The Table 2 provides how n and y impact shock dynamics and heat transfer. It is evident from Table 2 that, heat transfer effects are higher near the shock front, with heat loss tapering off as the flow travels away from the shock front. This data is useful for improving shock-induced heating systems, including those found in astrophysical plasmas, high-speed propulsion systems, and combustion chambers.

Table 2. Rate of heat transfer with respect to different values of n and y

y	n	Rate of heat transfer (Q^*)
0.5		-1.4122e+08
0.6		-1.4107e+08
0.7	-0.2	-1.4091e+08
0.8		-1.4073e+08
0.9		-1.4054e+08
0.5		-1.4141e+08
0.6		-1.413e+08
0.7	-0.3	-1.4118e+08
0.8		-1.4104e+08
0.9		-1.4089e+08
0.5		-1.4151e+08
0.6		-1.4142e+08
0.7	-0.4	-1.4132e+08
0.8		-1.412e+08
0.9		-1.4107e+08

Table 3 displays the frictional stress τ at various values of y for different values of n. From Table 3 it is clear that, shear stress is highest near the shock front, and diminishes with as one moves away from the shock front, which is consistent with boundary layer theory.

Table 3. Friction value with respect to different values of n and y

y	n	Friction (τ)
0.5	-0.2	-2.953711
0.6		-2.461872
0.7		-2.110918
0.8		-1.848201
0.9		-1.644525
1		-1.482429
0.5	-0.3	-2.651140
0.6		-2.209449
0.7		-1.894024
0.8		-1.657527
0.9		-1.473663
1		-1.326652
0.5	-0.4	-2.299816
0.6		-1.916544
0.7		-1.642786
0.8		-1.437475
0.9		-1.277795
1		-1.150058

5. Conclusions

This study investigated the combined effects of a magnetic field and multimodal heat transfer (conduction, convection, and radiation) on diverging spherical and cylindrical shock waves in an ideal magnetogasdynamics (MGD) medium. To the authors' knowledge, this study is the first comprehensive analysis of these coupled interactions, providing critical insights into nuclear explosions and high energy flow dynamics.

The key findings of the work are as follows;

- Convection induced significant variations in pressure and energy profiles, while velocity and density exhibited more stable trends. A reverse behavior in flow variables (v/v_b, ρ/ρ_b, p/p_b, F/F_b) was observed for $n = -0.3,\ -0.4$, highlighting convection's nonlinear influence. Specifically, parameter h^*modulated pressure and energy distributions significantly, confirming its importance in shock wave attenuation
- The magnetic field eliminated the sudden pressure peak p/p_b near the shock front causing a gradual decline that culminated in a vacuum state at an infinite distance from the shock. For $n = -0.4$, pressure and energy profiles grew faster, while density decayed more rapidly compared to the case with only the magnetic field effect.
- The coupling between shock dynamics and thermal transport exhibits strong geometric dependence. Cylindrical configurations promote axial heat/momentum redistribution, which (1) dampens flow reversal tendencies observed in spherical systems and (2) mitigates steep gradients through enhanced convective mixing. This results in more thermodynamically efficient energy transfer despite smoother flow profiles.

The study identified key areas for advancing shock wave research: relativistic effects in astrophysical flows, thermoelectric coupling in magnetized plasmas, and MHD boundary layer interactions. Extending the model to include viscous dissipation and chemical kinetics could further bridge theory with experimental observations in supersonic wind tunnels, hypersonic missiles, industrial shock tubes, next-generation propulsion systems, and inertial confinement fusion applications. These refinements would enhance predictive accuracy of shock wave propagation under extreme flow conditions.

Nomenclature

C	Dimensionless constant
C_a	Cowling number
e	Internal energy per unit mass [J/kg]
F	Total heat fluxes [W/m^2]
F_{Cd}	Conduction heat flux [W/m^2]
F_{Cn}	Convection heat flux [W/m^2]
F_{Rd}	Radiation heat flux [W/m^2]
h	Magnetic pressure [$Pa\ or\ \frac{N}{m^2}$]
h^*	Coefficient of convective heat transfer [$W/m^2.K$]
H^*	Dimensional constant
k	Gas's thermal conductivity coefficient [$\boldsymbol{W/m.K}$]
L	Characteristic length
M	Shock Mach number

n	Constant
N_u	Nusselt number
p	Pressure [$Pa\ or\ \frac{N}{m^2}$]
R^*	Universal gas constant [$J/K.mol$]
s	Space co-ordinate [m]
S_b	Shock radius [m]
S_p	Radius of the piston [m]
t	Time co-ordinate [s]
T	Absolute temperature [K]
v	Fluid velocity [m/s)
v_p	Piston velocity at $t = t_0$ [m/s]
W_f	Shock front speed [m/s]
y	Self-similarity variable
z^*	Step size

Greek symbols

α_R	Rosseland mean absorption coefficient
β	Density ratio
γ	Ratio of specific heat
ε	Dimensional constant
μ	Magnetic permeability [H/m]
ρ	Density of the fluid [kg/m^3]
σ	Stefan-Boltzmann constant [W/m^2K^4]
λ	Geometry of shock wave
φ	Increment function

Subscripts

$(.)_a$	Ahead of the shock front
$(.)_b$	Behind the shock front
$(.)_0$	Reference state

Acknowledgement

The authors would like to acknowledge the University Grant Commission (UGC), New Delhi, India, through the Savitribai Jyotirao Phule Fellowship for Single Girl Child (SJSGC) [F. No.82-7/2022 (SA-III)].

Funding Statement

This research did not receive any specific grant from funding agencies in the public, commercial, or not-for-profit sectors.

Conflicts of Interest

The author declares that there is no conflict of interest regarding the publication of this article.

Authors Contribution Statement

Kinakkal Athira: Conceptualization, Formal Analysis, Investigation, Methodology, Software, Validation, Visualization, Writing – Original Draft.

Dunna Narsimhulu: Conceptualization, Formal Analysis, Resources, Supervision, Visualization, Writing – Review & Editing.

Devarapalli Nagendra Prasad: Data curation, Resources, Visualization, Writing – Review & Editing.

References

[1] Lebedev, S. V., Frank, A., Ryutov, D. D., 2019. Exploring astrophysics-relevant magneto hydrodynamics with pulsed-power laboratory facilities. *Reviews of Modern Physics*, 91(2), p. 025002.

[2] Fomin, N. A., 2016. How the term “shock waves” came into being. *Journal of Engineering Physics and Thermophysics*, 89, pp. 1047–1065.

[3] Reichenbach, H., 1983. Contributions of Ernst Mach to fluid mechanics. *Annual Review of Fluid Mechanics*, 15(1), pp. 1–29.

[4] Guderley, K. G., 1942. Powerful spherical and cylindrical compression shocks in the neighbourhood of the center and of the cylindrical axis. *Luftfahrtforschung*, 19, p.302.

[5] Chester, W., 1954. CXLV. The quasi-cylindrical shock tube. *The London, Edinburgh, and Dublin Philosophical Magazine and Journal of Science*, 45(371), pp. 1293–1301.

[6] Chisnell, R. F., 1955. The normal motion of a shock wave through a non-uniform one-dimensional medium. *Proceedings of the Royal Society of London. Series A, Mathematical and Physical Sciences*, 232(1190), pp. 350–370.

[7] Whitham, G. B., 1958. On the propagation of shock waves through regions of non-uniform area or flow. *Journal of Fluid Mechanics*, 4(4), pp. 337–360.

[8] Gurovich, V. T., Grinenko, A., Krasik, Y. E., 2007. Semi-analytical solution of the problem of converging shock waves. *Physical Review Letters*, 99(12), p. 124503.

[9] Sharma, V. D., Arora, R., 2005. Similarity solutions for strong shocks in an ideal gas. *Studies in Applied Mathematics*, 114(4), pp. 375–394.

[10] Hafner, P., 1988. Strong convergent shock waves near the center of convergence: A power series solution. *SIAM Journal on Applied Mathematics*, 48(6), pp. 1244–1261.

[11] Van Dyke, M., Guttmann, A. J., 1982. The converging shock wave from a spherical or cylindrical piston. *Journal of Fluid Mechanics*, 120, pp. 451–462.

[12] Madhumita, G., Sharma, V. D., 2003. Propagation of strong converging shock waves in a gas of variable density. *Journal of Engineering Mathematics*, 46, pp. 55–68.

[13] Levin, V. A., Zhuravskaya, T. A., 1996. Propagation of converging and diverging shock waves under isothermal condition. *Shock Waves*, 6, pp. 177–181.

[14] Bertram, L. A., 1973. Magnetogasdynamics shock polar: Exact solution in aligned fields. *Journal of Plasma Physics*, 9(3), pp. 325–347.

[15] Singh, L. P., Singh, D. B., Ram, S. D., 2016. Growth and decay of weak shock waves in magnetogasdynamics. *Shock Waves*, 26, pp. 709–716.

[16] Marshak, R. E., 1958. Effect of radiation on shock wave behavior. *The Physics of Fluids*, 1(1), pp. 24–29.

[17] Bajargaan, R., Patel, A., 2017. Similarity solution for a cylindrical shock wave in a self-gravitating, rotating axisymmetric dusty gas with heat conduction and radiation heat flux. *Journal of Applied Fluid Mechanics*, 10(1), pp. 329–341.

[18] Nath, G., 2019. Cylindrical shock wave generated by a moving piston in a rotational axisymmetric non-ideal gas with conductive and radiative heat-fluxes in the presence of azimuthal magnetic field. *Acta Astronautica*, 156, pp. 100–112.

[19] Nath, G., Vishwakarma, J. P., 2014. Similarity solution for the flow behind a shock wave in a non-ideal gas with heat conduction and radiation heat-flux in magnetogasdynamics. *Communications in Nonlinear Science and Numerical Simulation*, 19(5), pp. 1347–1365.

[20] Vishwakarma, J. P., Nath, G., 2009. A self-similar solution of a shock propagation in a mixture of a non-ideal gas and small solid particles. *Meccanica*, 44, pp. 239–254.

[21] Laumbach, D. D., Probstein, R. F., 1970. Self-similar strong shocks with radiation in a decreasing exponential atmosphere. *The Physics of Fluids*, 13(5), pp. 1178–1183.

[22] Pomraning, G. C., 2005. *The Equations of Radiation Hydrodynamics*. Courier Corporation.

[23] Ghoniem, A. F., Kamel, M. M., Berger, S. A., Oppenheim, A. K., 1982. Effects of internal heat transfer on the structure of self-similar blast waves. *Journal of Fluid Mechanics*, 117, pp. 473–491.

[24] White, F. M., 1984. *Heat Transfer*. 1st ed. Addison Wesley Publishing Company.

[25] Zel'Dovich, Y. B., Raizer, Y. P., 2002. *Physics of Shock Waves and High-Temperature Hydrodynamic Phenomena*. Courier Corporation.

[26] Akbar, N. S., Mehrizi, A. A., Rafiq, M., Habib, M. B., Muhammad, T., 2023. Peristaltic flow analysis of thermal engineering nano model with effective thermal conductivity of different shape nanomaterials assessing variable fluid properties. *Alexandria Engineering Journal*, 81, pp. 395–404.

[27] Akbar, N. S., Akhtar, S., Maraj, E. N., Anqi, A. E., Homod, R. Z., 2023. Heat transfer analysis of MHD viscous fluid in a ciliated tube with entropy generation. *Mathematical Methods in the Applied Sciences*, 46(10), pp. 11495–11508.

[28] Akbar, N. S., Muhammad, T., 2023. Physical aspects of electro osmotically interactive cilia propulsion on symmetric plus asymmetric conduit flow of couple stress fluid with thermal radiation and heat transfer. *Scientific Reports*, 13(1), p. 18491.

[29] Jain, M. K., 1984. *Numerical Solution of Differential Equations*. New Age International (P) Ltd., Publishers, New Delhi.

[30] Musa, H., Saidu, I., Waziri, M. Y., 2010. A simplified derivation and analysis of fourth order Runge Kutta method. *International Journal of Computer Applications*, 9(8), pp. 51–55.

[31] Vats, V. K., Singh, D. B., Manjul, M., 2024. Similarity solution for the magnetogasdynamics shock waves in a self-gravitating and rotating ideal gas under the influence of radiation heat flux. *Physics of Fluids*, 36(7).

[32] Nath, G., Upadhyay, P., 2025. Analytical and numerical solution via group theoretic method for magnetogasdynamics shock wave under monochromatic radiation in non-ideal self-gravitating gas. *Journal of Nonlinear, Complex and Data Science*, 25(5–6), pp. 35–371.

[33] He, F., et al., 2023. Unsteady temperature distribution in a cylinder made of functionally graded materials under circumferentially-varying convective heat transfer boundary conditions. *Zeitschrift für Naturforschung A*, 78(10), pp. 893–906.

[34] Fehid, I., et al., 2024. Convective heat transfer with hall current using magnetized non-Newtonian Carreau fluid model on the cilia-attenuated flow. *International Journal of Numerical Methods for Heat and Fluid Flow*, 34(9), pp. 3328–3354.

[35] Rostami, S., et al., 2021. A study on the effect of magnetic field and the sinusoidal boundary condition on free convective heat transfer of non-Newtonian power-law fluid in a square enclosure with two constant-temperature obstacles using lattice Boltzmann method. *Journal of Thermal Analysis and Calorimetry*, 144, pp. 2557–2573.

[36] Ellahi, R., 2013. The effects of MHD and temperature dependent viscosity on the flow of non-Newtonian nanofluid in a pipe: Analytical solutions. *Applied Mathematical Modelling*, 37(3), pp. 1451–1467.